

Piezoelectrically Induced Diffraction Modulation of Light

L. TURI, Cs. KUTI, AND F. KRAUSZ

Abstract—A novel technique for efficient amplitude modulation of light is investigated: diffraction modulation by piezoelectrically induced standing wave refractive index gratings in photoelastic crystals. We describe the operation of such devices and derive expressions predicting the modulation efficiency in terms of material parameters and drive power. Experiments with a lithium niobate crystal have shown that 100% light modulation can easily be achieved with electrical powers of a few tens of milliwatts. Applying higher drive powers sharp transmission peaks are created. Owing to these unique features this technique is expected to significantly advance the state-of-the-art of actively mode-locked lasers.

I. INTRODUCTION

IT HAS been known for a long time that the strain-optic perturbation of the refractive index by piezoelectrically induced acoustic waves may severely affect the operation of wide-band electrooptic light modulators and switches [1], [2]. Nevertheless, the effect can also be turned to advantage in special cases when light modulation at discrete frequencies is to be accomplished. Weil and Halido [3] demonstrated orders of magnitude reduction of the half-wave voltage of an electrooptic modulator when driven at the piezoelectric resonance frequency of the crystal. They operated a bulk GaAs sample at its fundamental resonances of a few hundred kHz. A half-wave-retardation was achieved with voltages as low as a few volts. This technique allows efficient *phase* modulation of a collimated laser beam having a diameter much smaller than the acoustic wavelength in the crystal.

One of the most important application fields of modulators working at discrete frequencies is the active mode locking of lasers. This application, however, requires much higher modulation frequencies usually in the range of tens of MHz. Operation at the fundamental resonance in this range of the RF spectrum is possible only in very thin (waveguide) modulators with high insertion losses limiting their applications in laser cavities. This difficulty can be circumvented by driving a bulk sample at higher harmonic resonances. In this case modulation occurs by diffraction due to a phase grating rather than by a uniform

phase retardation of the light beam. The diffraction results in *amplitude* modulation of the transmitted (undeflected) beam provided that its diameter is much greater than the acoustic wavelength. The phase grating develops from acoustic standing waves which are generated on the faces of the resonance medium, unlike conventional acoustooptic modulators where the acoustic waves are injected by a transducer attached to the photoelastic material. Preliminary experiments using a lithium niobate (LiNbO_3) crystal revealed excellent modulation characteristics at low voltages [4].

In this paper we present a detailed analysis of diffraction modulation by the piezoelectrically induced strain-optic (PESO) effect. After reviewing the general principles of operation of standing-wave acoustooptic modulators we derive a simple relationship between drive power and modulation efficiency applying to both conventional and PESO devices. For the latter ones an elementary electrical characterization of piezoelectric resonators allows the evaluation of important material and resonator parameters from electrical measurements. The orientation dependence of the efficiency of PESO modulation can be analyzed by solving the acoustic wave equation containing the source term describing the piezoelectric excitation. Based on these calculations we have prepared a LiNbO_3 crystal sample and used it for experimental investigations. The results of the measurements are in good agreement with the predictions of the theory. Finally, the suitability of PESO diffraction modulation for active mode locking is briefly discussed.

II. PRINCIPLES OF OPERATION OF STANDING-WAVE MODULATORS

The index of refraction of a photoelastic material becomes perturbed when acoustic waves propagate in the medium [5]. In a crystal with two opposite plane parallel faces acoustic standing waves can be excited. The sound wave vector k_s is perpendicular to the faces of the acoustic resonator. The acoustic waves vary the index of refraction in a periodic manner forming a phase grating. This periodic index modulation results in diffraction of a laser beam traversing the crystal.

In the following we outline the theory of refractive index gratings in a form useful for the design of actual modulators. Let us suppose an acoustic standing wave to be oscillating in a crystal resonator. The displacement vector

Manuscript received October 23, 1989; revised March 12, 1990. This work was supported by the Fonds zur Förderung der wissenschaftlichen Forschung, Österreich, Austria, under project P 7282.

L. Turi and Cs. Kuti are with the Department of Experimental Physics, Technical University of Budapest, H-1521 Budapest, Hungary.

F. Krausz is with the IAEI, Technical University of Vienna, A-1040 Wien, Austria.

IEEE Log Number 9036230.

describing the sound wave can be written as

$$\mathbf{u}(\mathbf{r}, t) = qU_+ \sin(\omega_s t - \mathbf{k}_s \mathbf{r} + \varphi_+) + qU_- \sin(\omega_s t + \mathbf{k}_s \mathbf{r} + \varphi_-) \quad (1)$$

where \mathbf{q} is a unit vector in the direction of displacement, U_\pm and φ_\pm are amplitudes and phases of the waves propagating along the resonator axis, respectively, and ω_s is the angular sound frequency. The phases φ_\pm are chosen in such a way that U_\pm have positive values. From $\mathbf{u}(\mathbf{r}, t)$ the components of the strain tensor $S_{kl}(\mathbf{r}, t)$ can be derived [5]. Assuming a pure standing wave ($U_+ = U_-$) we obtain

$$S_{kl}(\mathbf{r}, t) = S_{kl} \sin(\omega_s t + \varphi_l) \sin(\mathbf{k}_s \mathbf{r} + \varphi_r) \quad (2)$$

with

$$S_{kl} = -(q_k s_l + q_l s_k) k_s U_+ \quad (3)$$

q_i and s_i are components of the unit vectors \mathbf{q} and $\mathbf{s} = \mathbf{k}_s/k_s$, where $k_s = 2\pi/\lambda_s = \omega_s/v_s$, λ_s is the sound wavelength and v_s is the sound frequency.

The photoelastic effect is traditionally described by $\delta B_{ij}(\mathbf{r}, t) = p_{ijkl} S_{kl}(\mathbf{r}, t)$, where $\delta B_{ij}(\mathbf{r}, t)$ represent the change of the impermeability tensor, and p_{ijkl} are the components of the strain-optic (photoelastic) tensor. Substituting $\delta B_{ij}(\mathbf{r}, t)$ into the equation of the optical indicatrix, the changed principal axes and the magnitude δn of the standing wave index grating can readily be calculated for any of the two polarization modes of an arbitrary propagation direction of light. δn generally takes the form

$$\delta n = f(B_{ij}, \delta B_{ij}, \mathbf{d}) \quad (4)$$

where $\delta B_{ij} = p_{ijkl} S_{kl}$ is the amplitude of the standing wave perturbation of B_{ij} , and \mathbf{d} is a unit vector along the direction of the electric displacement vector. The index grating is now described by (2), where the amplitude S_{kl} has to be replaced by δn . The magnitude of the phase grating is then given by

$$\delta\Phi = \frac{2\pi L}{\lambda} \delta n \quad (5)$$

where λ is the light wavelength in vacuum, and L is the interaction length in the crystal. We assume the light to propagate nearly normal to the acoustic wave vector, thus L is approximately equal to the thickness of the grating.

So far we have not been concerned with the origin of the acoustic wave. It can be injected into the resonant medium or created directly on its faces. Simple energy considerations allow a unified approach to the problem of acoustic wave generation in crystal resonators. The acoustic energy W_s stored in the medium must satisfy the equation

$$\frac{dW_s}{dt} = -\frac{W_s}{\tau_c} + \eta P \quad (6)$$

where $\tau_c = (\alpha_{\text{eff}} v_s)^{-1}$ is the cavity lifetime, and α_{eff} is the effective attenuation coefficient for the acoustic intensity including both the acoustic attenuation α_s in the res-

onant medium and the extrinsic resonator losses. $\alpha_{\text{eff}} d$ was assumed to be much smaller than unity, where d is the resonator length. The acoustic efficiency η is defined as the ratio of the acoustic dissipated power to P , the total power dissipation in the crystal. η takes its maximum value η_0 at resonance and goes to zero when the drive frequency is detuned from resonance. Electrical power dissipation due to the nonzero conductance of the transducer crystal generally causes η_0 to be less than one.

W_s is given by

$$W_s = V\rho\omega_s^2 U_+^2 \quad (7)$$

where $V = Lwd$ is the volume of the resonator (see, e.g., Fig. 4) and ρ is the mass density of the crystal. Introducing the quality factor $Q = \omega_s \tau_c$, the steady-state value of the acoustic wave amplitude may be expressed from (6) and (7) as

$$U_+ = \sqrt{\frac{\eta Q P}{V\rho\omega_s^3}} \quad (8)$$

Whereas in conventional standing-wave modulators η is a characteristic of the piezoelectric transducer, all the parameters appearing in (8) characterize the resonant medium in PESO devices. The parameters η and Q may be obtained from electrical measurements as shown in the next Section. At first sight, it seems to be surprising that elastic and piezoelectric constants do not appear in (8). Along with the dielectric constants they are comprised in η . Following from its definition, $\eta = 1$ in a piezoelectric medium free from dielectric losses, i.e., the steady-state amplitude of the acoustic standing wave does not depend on the actual value of the effective piezoelectric constant in this idealized case. In reality, there is always some electrical power dissipation, and η decreases with decreasing piezoelectric coefficient and crystal resistivity.

Analytic solutions to the problem of light diffraction by index gratings are obtained when the parameter $a = (2\pi/n)(\lambda L/\lambda_s^2)$ is much smaller or much greater than unity [6]. The two extreme cases are referred to as Raman-Nath (RN) and Bragg regime of optical diffraction, respectively. The practical limits of RN and Bragg diffraction may be taken as $a \leq 1$ and $a \geq 10$, respectively [7]. In a standing-wave modulator the intensity transmission for the zeroth-order (undeflected) light beam is given by

$$T_{\text{RN}}(t) = J_0^2(\delta\Phi \sin \omega_s t) \quad (9a)$$

in the RN regime, where J_0 is the zeroth-order Bessel function, and

$$T_{\text{BR}}(t) = \cos^2\left(\frac{\delta\Phi}{2} \sin \omega_s t\right) \quad (9b)$$

in the Bragg regime. We assumed that only one polarization mode is present in the crystal. Now, expressions (8), (3), (4), (5), and (9) provide a complete description of the modulation characteristics in terms of material and drive parameters. The intensity transmission functions are de-

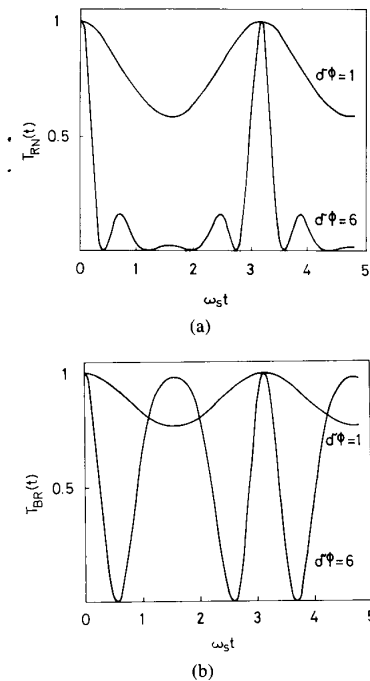


Fig. 1. Time-development of the zeroth-order transmitted light in the (a) Raman-Nath, (b) Bragg regime of optical diffraction for two different values of the magnitude of the phase grating.

picted in Fig. 1. For $\delta\Phi \leq 1$ the modulation is nearly sinusoidal in both cases, whereas for large amplitudes of the phase grating significant differences appear between the modulation characteristics of a Bragg and RN device. For $\delta\Phi \geq 2\pi$ the Bragg modulator opens twice or more during a modulation period whereas RN diffraction gives rise to single sharp transmission peaks when $\delta\Phi$ is increased. The intermediate region where $1 < a < 10$ is characterized by a mixture of features of the extreme cases discussed above.

The efficiency of light modulation by a standing wave diffraction modulator depends on the magnitude $\delta\Phi$ of the generated phase grating (also referred to as modulation depth). Although the detection of the time development of the modulator transmission gives direct information of $\delta\Phi$, it is usually more convenient to measure the ratio of the zeroth-order transmitted light power to that of the incident one averaged over one cycle:

$$\tau(\delta\Phi) = \frac{\omega_s}{2\pi} \int_0^{2\pi/\omega_s} T(\delta\Phi, t) dt \quad (10)$$

where $T(\delta\Phi, t)$ is one of the functions given by (9a) and (9b). Fig. 2 shows $\tau(\delta\Phi)$ for both operating regimes allowing a derivation of the modulation index $\delta\Phi$ from the measurement of τ .

III. ELECTRICAL CHARACTERIZATION OF A PIEZOELECTRIC RESONATOR

If the oscillation in an acoustic resonator is generated directly by the piezoelectric effect it is also called a pi-

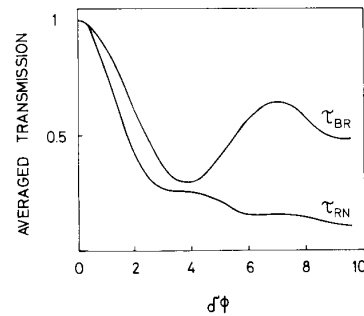


Fig. 2. Time-averaged transmission of the zeroth-order light beam as a function of the modulation depth $\delta\Phi$ for Raman-Nath diffraction and Bragg deflection.

ezelectric resonator. To characterize the behavior of this device from an electrical point of view equivalent electrical circuits are to be introduced. Exact circuit representations for crystal resonators usually have elements that are not ordinary frequency-independent inductors, capacitors, and resistors [8]. Approximate equivalent circuits are used to simplify the understanding of the electrical response of the crystal. One of the most frequently used approximate representation is the so called lumped-element circuit enclosed by the dashed line in Fig. 3. The series resonator consisting of the motional inductance L , the motional capacitance C , and the motional resistance R provides a satisfactory description of the electrical response of the acoustic resonator close to a particular resonance. Obviously, this treatment applies directly to a PESO modulator, whereas standing-wave modulators consisting of a separate piezoelectric transducer and interaction medium necessitate more complicated electrical circuit representations [9], which are not discussed here.

L , C , and R depend on the selected resonance frequency $\omega_r = 1/\sqrt{LC}$ and the physical properties of the crystal. C_0 is the "real" capacitance of the crystal including stray capacitances associated with the package and electrical leads, and R_0 accounts for the dielectric losses. The quality factor of the acoustic resonator introduced in the preceding section corresponds exactly to that of the series RLC oscillator in Fig. 3, thus $Q = L\omega_r/R$. Connecting an inductance L_0 parallel to the crystal so that $1/L_0C_0 = 1/LC = \omega_r^2$ a combination of a series and parallel oscillator is created with a single resonance frequency ω_r . This is a necessary step to realize impedance matching to a 50 Ω transmission line as we shall see below. The admittance of the created circuit near resonance can be written as

$$Y(r) \approx \frac{1 + 2jQ_0r}{R_0} + \frac{1}{R(1 + 2jQr)} \quad (11)$$

with $Q_0 = R_0/L_0\omega_r$, which is the quality factor of the parallel oscillator, $r = (\omega_s - \omega_r)/\omega_r$, and for $|r| \leq 1/Q_0$. $\omega_s = 2\pi\nu_m$, where ν_m is the modulator drive frequency. As R_0 and Q_0 are known from preliminary measurements made far from resonance, R and Q may be obtained from the measurement of Y near resonance. Making

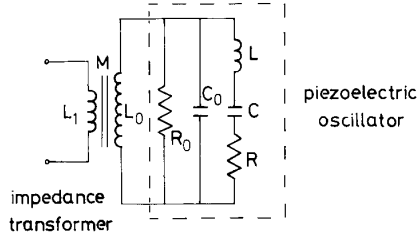


Fig. 3. Lumped-element equivalent circuit for a piezoelectric crystal oscillator with an impedance transformer providing impedance matching at resonance.

use of the definition of the acoustic efficiency we find from (11)

$$\eta(r) = \frac{1}{1 + (R/R_0) \sqrt{1 + 4(Qr)^2}} \quad (12)$$

where $r \ll 1$. At resonance, (12) gives

$$\eta_0 = \frac{R_0}{R + R_0}. \quad (13)$$

Thereby both η and Q are obtained from electrical measurements for the expressions derived in the preceding section.

Finally, impedance matching to a 50 Ω coaxial transmission line is realized by coupling a corresponding inductor L_1 to L_0 (the transformer is not represented by its equivalent circuit in Fig. 3). The input impedance of the circuit constructed in this way is $Z_{in} = (L_1/L_0) [RR_0/(R + R_0)]$ at resonance, where $M = L_0L_1$ was assumed. By appropriate choice of L_1 , $Z_{in} = 50 \Omega$ can be obtained.

IV. OPTIMUM CRYSTAL ORIENTATIONS FOR PESO DIFFRACTION MODULATION

The efficiency of PESO diffraction modulation may sensitively depend on the orientation of the acoustic resonator axis (s) with respect to the crystallographic axes due to the anisotropy of the piezoelectrical, acoustical, and optical properties of the crystal. This fact offers the possibility to optimize PESO diffraction by appropriate sample orientation. For this purpose a computer analysis of the orientation dependence of the PESO perturbation on the refractive index has been developed. The computer program is a modified version of a previous one used for the study of acoustic influences on the operation of electrooptic devices [2].

The analytical calculations are based on the differential equation describing bulk acoustic wave generation on the surface of a crystal by the piezoelectric effect [5]. To solve this equation we used the plane-wave ansatz (1) with $U_- = 0$, i.e., the wave created on the opposite face was disregarded. The acoustic attenuation was also left out of account in the calculations. U_+ was expressed for the different (shear, extensional) propagation modes as a function of the applied electric field, the piezoelectric and elastic tensor components, and the actual orientation of the crystal. Although the model is unable to describe

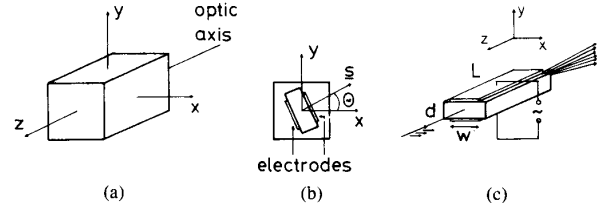


Fig. 4. (a)–(b) Acoustic resonator orientation defined by the angle Θ between the resonator axis and the crystallographic x -axis of the LiNbO_3 sample. (c) Optimum orientation for PESO diffraction modulation in LiNbO_3 .

standing-wave operation at cavity resonance, it is very useful for the selection of appropriate materials and finding optimum crystal orientations for efficient PESO generation of standing-wave refractive index gratings.

A LiNbO_3 crystal sample has been chosen for our investigations because of its high piezoelectric and photoelastic constants, excellent optical quality, and low acoustic attenuation. We restricted our investigations to optic axis light propagation in LiNbO_3 . Therefore, we sought the optimum sound propagation direction in the xy plane (see Fig. 4). The angle Θ formed by s and the x axis was used as a parameter of orientation as shown in Fig. 4(b). The strain-optic effect causes the index ellipsoid to be rotated. In the special case when s lies in the xy plane two major axes remain approximately in the xy plane. The periodic variation of these axes is responsible for the diffraction of light sent through the crystal along the z axis.

To characterize the strength of the strain-optic perturbation with a single quantity, the birefringence $\Delta n_{SO} = \Delta n_1 - \Delta n_2$ was computed first, where $\Delta n_{1,2}$ are the amplitudes of periodic index variations caused by one of the two acoustic waves arising from the electrode faces, and the subscripts refer to the major axes of index ellipsoid lying in the xy plane [10], [11], [12]. Δn_{SO} is normalized to the electrooptically induced birefringence Δn_{EO} by the same electric field. The ratio $\Delta n_{SO}/\Delta n_{EO}$ is shown by the lower traces in Fig. 5(a) as a function of Θ for the extensional (E) and shear (S_1, S_2) waves. The upper traces in Fig. 5(a) represent the phase velocities, which are depicted for later reference. The displacement vectors of the shear waves S_1, S_2 are parallel and normal to the z axis, respectively.

The 3 m crystallographic point group has a three-fold axis of rotational symmetry ($2C_3$), which coincides with the optic axis of LiNbO_3 . As a consequence, Θ scans a range between 0 and 120° in Fig. 5. The computations predict appreciable birefringence induced by the PESO effect for the shear wave S_1 and for the extensional wave. Although the shear wave S_1 produces the strongest photoelastic effect according to our calculations, recent experimental investigations showed that the most efficient PESO standing wave diffraction is achieved with the extensional wave. This paradox can be resolved by taking into account the different attenuations of the two acoustic modes.

To find the optimum Θ and light polarization direction

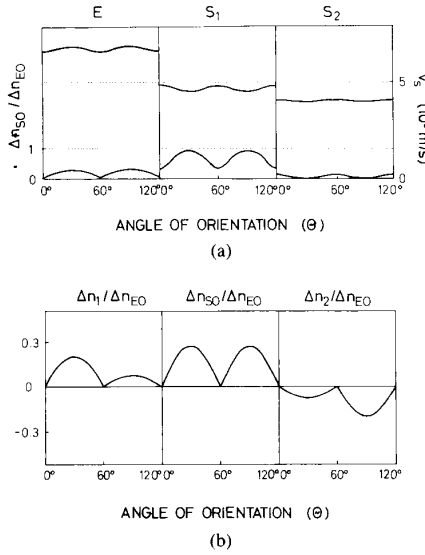


Fig. 5. Acoustic and optical characteristics of extensional (E) and shear (S_1 , S_2) waves as a function of the angle of orientation Φ . (a) The upper traces are phase velocities (v_s) of the different modes. The lower traces represent the ratio of the strain-optically and electrooptically induced birefringence ($\Delta n_{SO}/\Delta n_{EO}$). (b) The change in refractive indices due to the extensional wave along the main axes of the index ellipsoid in the crystallographic xy plane.

for PESO diffraction, Δn_1 and Δn_2 are depicted in Fig. 5(b) for the extensional wave. The strongest effect occurs at $\theta = 30^\circ$ and $\theta = 90^\circ$ along one and the other index axis, respectively. For the sake of simpler theoretical description we chose $\theta = 90^\circ$ in our experiments. In this case s and thus the resonator axis coincides with the y axis of the crystal and the directions of the major axes of the index ellipsoid happen to remain nearly unchanged. As a consequence, the traversing light has to be polarized parallel to the x axis of the crystal, as shown in Fig. 4(c). For this special orientation (3) simplifies to

$$S_2 = -2k_s U_+ \quad (3')$$

and (4) takes the form

$$\delta n = -\frac{n_o^3}{2} p_{12} S_2 \quad (4')$$

where contracted indexes are used to denote the tensor components [5], and n_o represents the ordinary index of refraction. Equations (3'), (4'), and (8) yield upon substitution in (5):

$$\delta\Phi = \frac{L}{\lambda} n_o^3 p_{12} \sqrt{2\pi\eta Q} \sqrt{\frac{P_{RF}}{V v_m Q v_s^2}} \quad (5')$$

Expressions (5'), (9), and (10) enable us a straightforward comparison between experimental results and theoretical predictions.

V. EXPERIMENTS

The LiNbO₃ crystal used in the experiments is shown in Fig. 4(c). The dimensions of the acoustic cavity were

$L = 24$, $d = 3$, and $w = 4$ mm. Beside the aperture faces normal to the z axis those normal to the y axis were also polished optically flat and additionally parallel to within 5 s of arc, in order to assure a high Q of the acoustic resonator. Aluminium electrodes were evaporated on the xz faces of the sample. The crystal was driven at the 33th harmonic of the extensional wave at $\nu_r = \omega_r/2\pi = 33.02$ MHz.

First, we investigated the electrical properties of the piezoelectric oscillator. The capacitance C_0 far from resonance was calculated to be $C_0 \approx 13$ pF, where $\epsilon_{11}^S = 0.39 \times 10^{-9}$ F/m was used [11]. This value of C_0 with a loss tangent of $\tan \delta \approx 0.17$ at ≈ 33 MHz yielded $R_0 \approx 2.3$ k Ω . The appended parallel resonator had a quality factor of $Q_0 = (\tan \delta)^{-1} = 5.9$. We measured the admittance of this circuit given by (11), in the vicinity of ω_r . The peak value and the resonance width at half maximum were found to be ≈ 3.8 mS and ≈ 0.9 kHz, respectively. These numbers result in $R \approx 0.3$ k Ω , $Q \approx 1.1 \times 10^5$ and $\eta_0 = 0.88$. The obtained value of Q is in good agreement with early experimental results [13].

Optical measurements were performed with a He-Ne laser (633 nm) and with a CW Nd:glass laser (1054 nm) [14]. The light beam was sent through the crystal along the optic axis and was polarized parallel to the x axis as shown in Fig. 4(c). The laser beam was diffracted due to the acoustic phonons propagating in the y direction. A typical diffraction pattern at $\lambda = 633$ nm is shown in Fig. 6. With the 5 mW output of the He-Ne laser multiple scattering up to the 13th order of diffraction was observed by the unaided eyes when the crystal was driven with 1 W. From the diffraction angle we obtained the sound velocity to be $v_s = 6780$ m/s, which compares fairly well with the theoretical value of 6870 m/s [see Fig. 5(a)].

With this value the sound wavelength at 33 MHz is $\lambda_s = 205$ μ m, which yields $a = 0.98$. As a consequence, at $\lambda = 633$ nm the modulator works in the RN regime, i.e., (9a) may be used to describe the modulation characteristics. For $\lambda = 1054$ nm $a = 1.64$, i.e., the diffraction is still close to the RN regime.

Screening off the scattered light the time-averaged transmission τ was measured by a slow photodiode. The closed and open circles in Fig. 7 represent the experimental results for $\lambda = 633$ nm and $\lambda = 1054$ nm, respectively. (5'), (9a), and (10) provide a theoretical description for the experiment. We chose the product ηQ as a fit parameter and fitted $\tau(\eta Q, P)$ to the measured data at $\lambda = 633$ nm. With $\eta Q = 4.1 \times 10^4$ excellent agreement was achieved between theory and experiment at this wavelength. $\tau(\eta Q, P)$ is depicted also for $\lambda = 1054$ nm using the same value of ηQ . The agreement is still quite satisfactory inspite of the increased value of the parameter a . The electrical measurements yielded $\eta_0 Q = 9.7 \times 10^4$. The discrepancy may be attributed partly to the inaccuracy of the photoelastic constant [15], and indirectly to the nonzero temperature coefficient of the resonance frequency as we shall see later.

Fig. 7 shows that 100% modulation can be achieved at

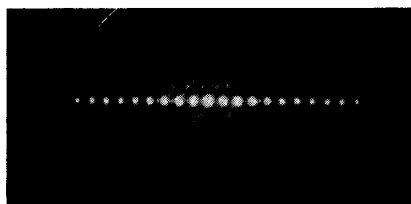


Fig. 6. Multiple scattering by Raman-Nath diffraction at a light wavelength of 633 nm when the modulator was operated at $\nu_m \approx 33$ MHz, and $P \approx 1$ W.

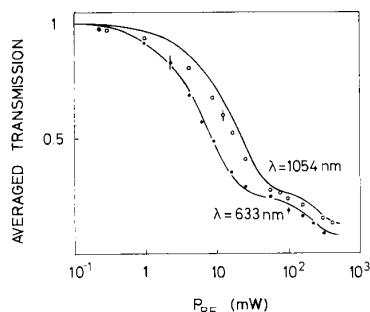


Fig. 7. Time-averaged transmission τ_{RN} of the LiNbO₃ sample as a function of the dissipated RF power. The full and open circles represent experimental data measured at 633 nm and 1054 nm, respectively. They are normalized to the transmission of the device turned off. The curves are theoretical fits obtained by the procedure described in the text.

both wavelengths with drive powers as low as a few tens of milliwatts. To make sure of the conclusions concerning the modulation depth, the transmitted light was detected with a fast photodiode. Oscilloscope traces are shown in Fig. 8. The bandwidth of the detection system was 400 MHz. The measurements were carried out at a drive power of $P \approx 100$ mW. The undeflected light was subjected to a sharp modulation at both wavelengths. The traces clearly reveal the modulation characteristics predicted by (9a). The transmission peaks are broader at $\lambda = 1054$ nm due to a reduced $\delta\Phi$ according to (5). The peak transmission corresponds to that without modulation giving evidence of pure standing-wave generation without any traveling-wave component.

The temperature coefficient of the resonance frequency was measured to be $\partial\nu_r/\partial T = -3.7$ kHz/°C. As the resonance width is less than 1 kHz, the crystal temperature must be stabilized to within a fraction of 1°C. To maintain long-term stability of the modulation, a simple temperature control circuit has been constructed. However, stable operation could not be achieved at the peak and the negative side of the resonance curve even with this temperature feedback-control. By contrast, stable operation was easily obtained when tuning the drive frequency from higher values towards resonance. This points to an efficient self-stabilization mechanism on the positive side of the resonance curve due to the negative temperature coefficient $\partial\nu_r/\partial T$. As a result, highly stable operation over a long time scale could be achieved at the expense of a somewhat reduced η . The stability was not affected by increasing the drive power well above 1 W.

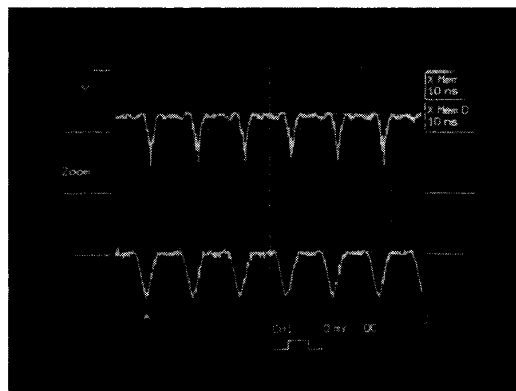


Fig. 8. Time development of the zeroth-order beam transmitted by the LiNbO₃ PESO modulator. The lower and upper traces were measured at 1054 nm and 633 nm, respectively, when the sample was driven at $P_{RF} \approx 0.1$ W. One division corresponds to 10 ns. The signals are somewhat noisy due to the limited bandwidth of our digital oscilloscope.

Rotating the light polarization by 90° considerably reduced the diffraction efficiency, confirming our theoretical predictions [Fig. (5b)]. It was interesting to compare the efficiencies of diffraction by the extensional and shear waves. We found that in spite of the predictions of the computer calculations, diffraction by the shear wave S_1 was significantly weaker than that by the extensional wave. The reason for this behavior is the higher acoustic attenuation for shear than for extensional waves in LiNbO₃ [16]. In fact, the resonance width for the S_1 mode turned out to be several kHz indicating a reduced Q factor in comparison with that of the extensional mode.

VI. CONCLUSION

The capabilities of PESO diffraction modulators for the purpose of mode locking can be analyzed using the theory of amplitude-modulation (AM) mode locking [17]. This yields for the steady-state pulse duration in a continuous wave (CW) mode-locked laser: $\tau_p \sim (\delta\Phi\nu_m)^{-1/2}$. The modulation depth $\delta\Phi$ is a key parameter for the production of short pulses. Consequently, efficient ultrashort pulse generation is expected by the PESO modulator presented in this paper due to its very high modulation depth. The theory predicts $\tau_p \approx 30$ ps for a CW Nd:YAG laser when mode locked by our PESO modulator driven at $\nu_m \approx 50$ MHz with $P \approx 1$ W. Self-phase-modulation in the active medium may reduce this pulse duration below 20 ps [18]. Considerably shorter pulses are expected from a Nd:glass laser. In fact, we succeeded in the generation of 4 ps pulses by PESO mode locking of a CW Nd:glass laser recently. Along with a detailed analysis of mode locking by standing-wave modulation, these experiments have been the subject of a recent publication [19].

At low (and moderate) modulation frequencies ($\nu_m < 100$ MHz) the attenuation in acoustic resonators is usually dominated by extrinsic cavity losses [19], [20], which may be significantly lower in PESO devices than conventional standing-wave modulators. This is why much higher modulation depths can be achieved by PESO diffraction

than traditional acoustooptic modulation at moderate frequencies. Commercially available Bragg-modulators, which are the most widely used for AM mode locking, produce modulation depths of the order of unity at $P \approx 1$ W. Our experiments yielded $\delta\Phi = \gamma\sqrt{P}$ with $\gamma(633 \text{ nm}) = 18.3$ and $\gamma(1054 \text{ nm}) = 11.2$, where P is given in watts. Beside the much higher modulation depths PESO standing-wave modulators have further advantages over traditional acoustooptic devices: 1) The monolithic construction eliminates the involved technological processes of transducer fabrication and acoustic bonding, and allows the device to be driven at significantly higher RF powers. 2) Simple exchange of the impedance transformer makes operation in a wide range of modulation frequencies from tens to hundreds of MHz possible. These features open attractive prospects for application of PESO diffraction modulators in actively mode-locked lasers.

ACKNOWLEDGMENT

The authors are grateful to Prof. A. J. Schmidt for his stimulating support. Cs. Kuti wishes to thank helpful discussions with Prof. C. H. Lee.

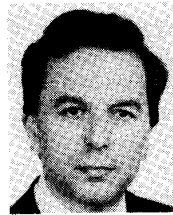
REFERENCES

- [1] F. Hoff and B. Stadnik, "Effects of piezoelectric resonances in ADP and KDP light-modulator crystals," *Electron. Lett.*, vol. 2, p. 293, 1966.
- [2] Cs. Kuti, Thesis, Hungarian Academy of Sciences, Budapest, 1984.
- [3] R. Weil and D. Halido, "Resonant piezoelectro-optic light modulation," *J. Appl. Phys.*, vol. 45, pp. 2258-2265, 1974.
- [4] Cs. Kuti, L. Turi, L. Yan, and C. H. Lee, "High efficiency diffraction modulation of light by standing acoustic waves from piezoelectrically induced strain-optic effect in LiNbO_3 ," in *Proc. OSA 1989 Annu. Meet.* Paper MG5.
- [5] J. Sapriel, *Acousto-Optics*. New York: Wiley, 1979.
- [6] N. Uchida and N. Niizeki, "Acoustooptic deflection materials and techniques," *Proc. IEEE*, vol. 61, pp. 1073-1092, 1973.
- [7] W. R. Klein and B. D. Cook, "Unified approach to ultrasonic light diffraction," *IEEE Trans. Sonics Ultrason.*, vol. SU-14, pp. 123-134, 1967.
- [8] T. R. Meeker, "Acoustic resonators and filters," in *Precision Frequency Control*, vol. 1, E. A. Gerber and A. Ballato, Eds. Orlando, FL: Academic, 1985.
- [9] G. S. Kino, *Acoustic waves: Devices, Imaging, and Analog Signal Processing*. Englewood Cliffs, NJ: Prentice-Hall, 1987.
- [10] The elastic (c_{ij}^E), piezoelectric (e_{ij}), and dielectric (ϵ_{ij}^S) constants were taken from [11], whereas the components of the strain-optic (p_{ij}) and electrooptic (r_{ij}^S) tensor were taken from [12].
- [11] R. T. Smith and F. S. Welsh, "Temperature dependence of the elastic, piezoelectric, and dielectric constants of lithium tantalate and lithium niobate," *J. Appl. Phys.*, vol. 42, pp. 2219-2230, 1971.
- [12] A. Yariv and P. Yeh, *Optical Waves in Crystals*. New York: Wiley, 1984.
- [13] E. G. Spencer, P. V. Lenzo, and K. Nassau, "Elastic wave propagation in lithium niobate," *Appl. Phys. Lett.*, vol. 7, pp. 67-69, 1965.
- [14] F. Krausz, E. Wintner, A. J. Schmidt, and A. Dienes, "Continuous wave thin plate Nd:glass laser," *IEEE J. Quantum Electron.*, vol. 26, pp. 158-168, Jan. 1990.
- [15] We used the photoelastic constant p'_{12} corrected for the piezoelectric effect: $p'_{12} = p_{12} + r_{22}^S e_{22} / \epsilon_{22}^S = 0.11$.
- [16] J. Reintjes and M. B. Schulz, "Photoelastic constants of selected ultrasonic delay-line crystals," *J. Appl. Phys.*, vol. 39, pp. 5254-5258, 1968.
- [17] D. J. Kuizenga and A. E. Siegman, "FM and AM mode-locking of the homogeneous laser—Part I," *IEEE J. Quantum Electron.*, vol. QE-6, pp. 694-715, 1970.
- [18] F. Krausz, T. Brabec, E. Wintner, and A. J. Schmidt, "Mode locking of a continuous wave Nd:glass laser pumped by a multistripe diode laser," *Appl. Phys. Lett.*, vol. 55, pp. 2386-2388, 1989.
- [19] F. Krausz, L. Turi, Cs. Kuti, and A. J. Schmidt, "Active mode locking of lasers by piezoelectrically induced diffraction modulation," *Appl. Phys. Lett.*, vol. 56, pp. 1415-1417, 1990.
- [20] B. A. Auld, *Acoustic Fields and Waves in Solids*. New York: Wiley, 1973.



L. Turi was born in Cegled, Hungary in 1960. He received the M.S. degree in physics from the Kossuth Lajos University, Debrecen in 1985.

Since 1987 he has been with the Technical University of Budapest. He is a lecturer of physics at the Department of Experimental Physics. His main research field is the investigation of ferroelectric crystals.



Cs. Kuti received the M.S. degree in physics from the Eötvös Roland University, Budapest, Hungary, the Ph.D. degree in applied physics from the Technical University of Budapest and the Candidate of Physics degree from the Hungarian Academy of Sciences in 1961, 1969, and 1984, respectively.

Since 1963 he has been with the Technical University of Budapest, and is currently an associate professor with the Department of Experimental Physics. He has worked on a variety of problems in solid-state physics. Recently his research interests center on nonlinear optical phenomena in crystals and control of laser radiation.

F. Krausz, for a photograph and a biography, see p. 168 of the January 1990 issue of this JOURNAL.